**Omega-P R&D, Inc.**
291 Whitney Avenue, Suite 401
New Haven, CT 06520

# MULTI-MODE CAVITY ACCELERATOR STRUCTURE

SBIR FY2015 Phase I Release 2 grant DE-SC0013886
Topic 26a: ADVANCED CONCEPTS AND TECHNOLOGY FOR PARTICLE ACCELERATORS
*Advanced Accelerator Concepts and Modeling*

J. L. Hirshfield, Principal Investigator
tel: (203) 789-1164, e-mail: jay.hirshfield@yale.edu

## FINAL REPORT

***Abstract*** **-** This project aimed to develop a prototype for a novel accelerator structure comprising coupled cavities that are tuned to support modes with harmonically-related eigenfrequencies, with the goal of reaching an acceleration gradient >200 MeV/m and a breakdown rate $<10^{-7}$/pulse/meter. Phase I involved computations, design, and preliminary engineering of a prototype multi-harmonic cavity accelerator structure; plus tests of a bimodal cavity. A computational procedure was used to design an optimized profile for a bimodal cavity with high shunt impedance and low surface fields to maximize the reduction in temperature rise $\Delta T$. This cavity supports the $TM_{010}$ mode and its 2nd harmonic $TM_{011}$ mode. Its fundamental frequency is at 12 GHz, to benchmark against the empirical criteria proposed within the worldwide High Gradient collaboration for X-band copper structures; namely, a surface electric field $E_{sur}^{max} < 260$ MV/m and pulsed surface heating $\Delta T^{max} < 56$ °K. With optimized geometry, amplitude and relative phase of the two modes, reductions are found in surface pulsed heating, modified Poynting vector, and total RF power—as compared with operation at the same acceleration gradient using only the fundamental mode.

CONTENTS



This report was written by Dr. Yong Jiang, Research Scientist at Yale University and consultant to Omega-P R&D, Inc., and by Dr. J. L. Hirshfield, Principal Investigator and Scientific Director at Omega-P R&D, Inc. Significant contributions to the project were made by Omega-P R&D research scientist Dr. Sergey V. Shchelkunov

April 5, 2016

## I. INTRODUCTION

Topic 26a in the DoE SBIR/STTR FY2015 Release 2 Program Solicitation sought Phase I proposals "…to develop new or improved accelerator designs that can provide very high gradient (>200 MV/m for electrons) acceleration of intense bunches of particles…..For all proposed concepts, stageability, beam stability, manufacturability, and high-wall-plug-to-beam power efficiency must be considered." In response, a proposal was submitted by Omega-P, R&D Inc., and awarded as grant DE-SC0013886. The project aim is to develop in Phase I (and demonstrate in Phase II) a prototype of a novel accelerator structure comprising coupled cavities that are tuned to support modes with harmonically-related eigenfrequencies, with the goal of reaching an acceleration gradient >200 MeV/m and a breakdown rate $<10^{-7}$/pulse/meter. Here we report on the Phase I work that is intended to lead to a Phase II project for reaching the above goal.

Normal conducting RF technology has been employed for decades in accelerators for discovery science and applications. A collaboration between SLAC, CERN, and KEK has moved towards reliable high acceleration gradient operation, achieving a 100 MV/m gradient for a CLIC X-band structure, with the goal of reaching an RF breakdown rate $\leq 10^{-7}$/pulse/meter. Improved understanding of RF breakdown mechanisms, and their dependencies upon material properties and fabrication procedures have led to predictions that room-temperature X-band linacs will able to operate at gradients up to 175 MV/m with low breakdown rates. This prediction is based on extrapolating data from cavity tests at the SLAC RF-breakdown test facility [1], as shown in Fig. 1.

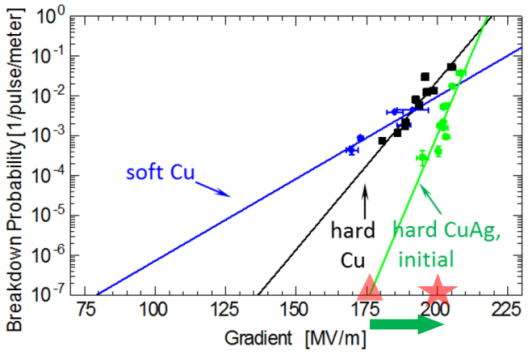


**Fig. 1**: Breakdown data for three SLAC 1C-SW-A2.75-T2.0-structures made of soft heat treated Cu, hard Cu and hard CuAg, with 150 ns shaped pulses [1]. These data suggest that a hard CuAg alloy structure can operate at 175 MV/m (indicated by triangle) with a breakdown rate $<10^{-7}$/pulse/meter. The goal proposed here is to push towards 200 MV/m (indicated by star) without increasing the breakdown rate.

In general, scaling laws suggest that higher frequency operation could allow even higher gradients. For example, a Ka-band structure is predicted operate at a gradient >200 MV/m, and in W-band at ~1 GV/m with much shorter filling time [2]. But the absence of suitable RF sources prevents direct tests of these predictions. This limitation can be overcome using beam-driven excitation of a cavity or accelerator structure. In fact, recent SLAC RF breakdown tests of a short mm-scale structure were carried out at FACET using single-bunch excited mm-wave wake fields; a maximum accelerating gradient of 0.3 GV/m without breakdown was inferred in the frequency range 115 to 140 GHz [3]. These SLAC experiments were limited by available FACET beam time, and by use of single-bunch beams. In our present proposal, tests of lower frequency externally-driven accelerator structures are proposed—but still to reach a gradient approaching 200 MV/m—by using cavities with a harmonic frequency mode operating together with the fundamental mode, which we predict can be done while maintaining a low RF-breakdown rate.

Phase I involved computations, design, and preliminary engineering of a prototype multi-harmonic cavity (MHC) accelerator structure; plus tests of a bimodal cavity. The goals for a follow-on Phase II project are to build the structure and conduct proof-of-principle experiments with it, using drive power from a unique RF source at the Yale Beam Physics Lab to supply multi-MW mutually-phase-coherent power at 2.856 and 5.712 GHz.

## II. TECHNICAL APPROACH

For future progress in high energy physics, a multi-TeV linear accelerator is desired to explore the energy frontier beyond that which can be reached by LHC [4]. But RF breakdown appears to be a major hurdle preventing warm accelerator structures from reaching high gradients [4]. Any mechanism that shows promise for obtaining lower RF breakdown probability at higher acceleration gradient is of great interest to the accelerator physics community. R&D within the US High Gradient Collaboration to study RF breakdown has been long underway [5]. But there remain deficiencies in fundamental understanding of the phenomena underlying RF breakdown. Work reported here is of for design of test structures embodying microwave cavities that support two modes, with the higher mode's eigenfrequency equal to a harmonic of that of the fundamental $TM_{010}$ mode. Future experiments will aim to systematically demonstrate the feasibility of applying several RF-breakdown-suppression mechanisms which we predict could lead to improved design of warm structures with higher accelerator gradients and lower breakdown probabilities than can be achieved using comparable single-cavity-mode structures. This work is intended to be a timely follow-on to that initiated by DoE in September 2014 with award of a modest four-year grant (1.5 FTE) to Yale University under grant DE-SC-00010699 for design and tests of individual bimodal cavities to sustain high acceleration gradients while minimizing breakdown rates. Design of accelerator structures comprising such cavities requires considerable additional work arising from need for external couplers at two frequencies and need to optimize tunings of each cavity at two frequencies in the presence of couplings between adjacent cavities; those issues are among the tasks reported on here

A main motivation for introducing a harmonic frequency component to cavity fields is to suppress pulsed heating and lower the modified Poynting vector [6] in expectation of suppressing RF breakdown**.** We take the superposition of RF *E*-fields in an accelerator cavity to be given by $E_{total} = (1-\alpha)E_1 + \alpha E_2$, where $E_{1,2}$ is each electric field component with acceleration gradient normalized to the same value, and where $\alpha$ is the percentage of the 2nd mode such that $E_{total}$ also provides the same acceleration gradient. Similarly the RF *H*-field is taken to be $H_{total} = (1-\alpha)H_1 + \alpha H_2$. As a result, the surface pulsed heating temperature rise $\Delta T$ can be scaled approximately in terms of the surface magnetic fields $H_1$ and $H_2$ as

$$\Delta T \propto (1-\alpha)^2 < H_1^2 > +\alpha^2\sqrt{f_2/f_1} < H_2^2 > = [(1-\alpha)^2 + \alpha^2\eta^2] < H_1^2 >,$$

where the quantity $\sqrt{f_2/f_1}$ arises from the surface resistivity, where $\eta = \sqrt{(f_2/f_1)^{1/2} < H_2^2 > / < H_1^2 >}$, and where the cross term averages out over each cycle. Due to the quadratic dependence of $\Delta T$ upon $\alpha$, it is possible to choose an optimal $\alpha$ such that $(1-\alpha)^2 + \alpha^2\eta^2 < 1$, i.e., to have lower temperature rise than for a single mode alone, keeping the same acceleration gradient. This is shown quantitatively in Fig. 2. The modified Poynting vector $S_c$ [6], and total required RF power $P_{tot}$, also follow a quadratic dependence on $\alpha$, so use of two modes is expected to lower these and pulsed temperature rise as well.

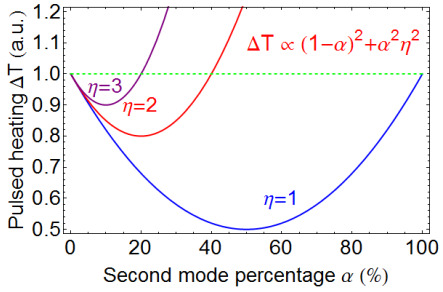


**Fig. 2:** Dependence of the surface pulsed heating temperature rise $\Delta T$ on 2nd mode fraction $\alpha$. There is seen to be a range of $\alpha$ within which $\Delta T$ can be smaller than for a single mode (the green dashed line).

However, for a pillbox-like cavity form designed as a bimodal cavity with a typical iris size of $0.1\lambda$ – $0.2\lambda$, our analysis shows that $\eta > 3$. This implies that $\Delta T$ would decrease by less than 10% through use of such a pillbox. As a result, a computational procedure has been used to design an optimized profile for a bimodal cavity to maximize the reduction in temperature rise $\Delta T$. To this end, a software package has been developed by us to optimize cavity geometry to support multi-harmonic modes with desired RF properties, such as high shunt impedance and low surface fields. This code is implemented in

*Mathematica* with a graphic user interface to provide real-time updates of 2D mesh, surface field and shunt impedance estimations while manually adjusting initial control points. It integrates *Finite Element Method* and *Generic Algorithm*, so that it can find global optimization of RF parameters by varying control points after an initial geometry is inputted. It solves for the field patterns of multiple eigenmodes simultaneously to allow optimization of the field amplitude relationship between different modes. It also allows periodic boundary conditions to be imposed to find eigenmode solutions for travelling wave structures. Currently the code package is being extended to include beam-cavity interactions to allow multipactor, wakefield and beam dynamics studies to be carried out in our unconventional structures.

Optimization of design for a bimodal cavity supporting the $TM_{010}$ mode and its 2nd harmonic $TM_{011}$ mode can be realized using this code package, as shown in Fig. 3. The figure shows a full $\pi$-mode accelerating cavity with its iris and beam pipe opening. Its fundamental frequency is at X-band (12 GHz), to benchmark against the empirical criteria recently proposed within the worldwide High Gradient collaboration for X-band copper structures [6,7]; namely, a surface electric field $E_{sur}^{max} < 260$ MV/m and pulsed surface heating $\Delta T^{max} < 56$ °K. With our optimized geometry shown in Fig. 3 the benefits of reducing surface pulsed heating, modified Poynting vector, and total RF power are evident, as shown in Fig. 4, Fig. 5 and Table 1. In Fig. 5, the pulsed heating temperature rise in our bimodal superposition can be 32% smaller than that in the fundamental mode alone for the same cavity; and the maximum magnitude of modified Poynting vector $S_c$ can be lower by 20%, with a 22% 2nd harmonic component and the relative phase of 90° between the two modes (Both modes are then in sychronization phase when this bimodal cavity is operated as an accelerating cavity). The peak surface *E*-field is the same as that of the fundamental mode due to this phase relationship, and no *anode-cathode effect* [8] is present. Note that even for the single $TM_{010}$ mode, $S_c$ is small due to the reduced *H*-field around the iris.

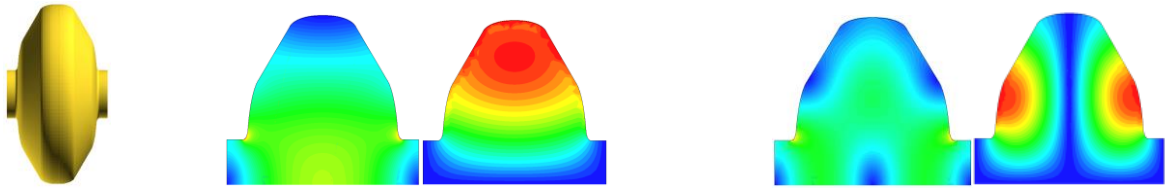

(a) (b) (c)

**Fig. 3:** (a) Preliminarily optimized bimodal cavity; Electromagnetic field pattern of (b) $TM_{010}$ and (c) its 2nd harmonic $TM_{011}$, left: *E*-field, right: *H*-field.

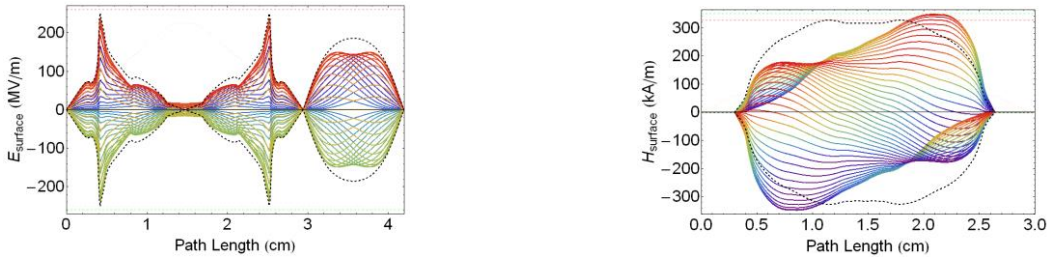


(a) (b)

**Fig. 4:** (a) surface *E*-field and (b) surface *H*-field along the cavity periphery at different times for superposition of $TM_{010}$ and $TM_{011}$, where the dotted line indicates fields of single mode $TM_{010}$. *H*-field asymmetry is due to field distribution and phase choice of $TM_{011}$.

In Table 1, RF parameters for this bimodal cavity are listed together with other cavity configurations. Although the instantaneous surface *H*-field is increased, the pulsed heating temperature rise is the lowest since the exposure time to the peak *H*-field is shortened, and temperature rise is a time-averaged effect and is quadratically dependent on the mode percentage $\alpha$ in our two-mode superposition. The total RF power is reduced, while maintaing the same acceleration gradient, so its effective shunt impedance is much increased. Together with shorter filling time for the 2nd harmonic component, the RF-to-beam efficiency can be improved, as will be discussed below.

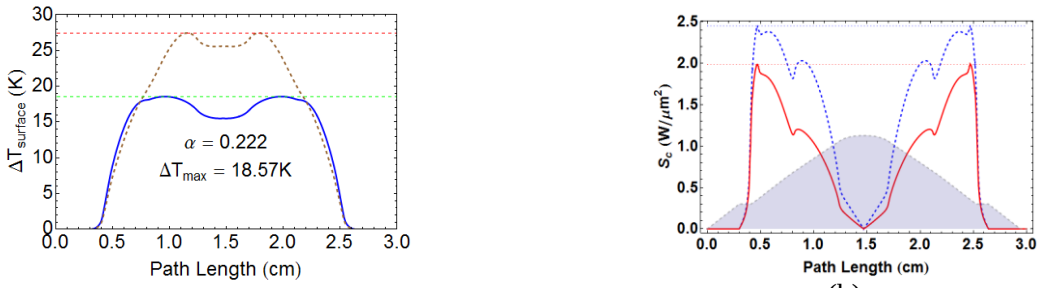


(a) (b)

**Fig. 5:** (a) Optimized maximum pulsed heating temperature rise (blue line) is 18.57 °K, compared to that of single mode 27.5 °K (brown dotted line) with a 200 ns pulse width; (b) maximum modified Poynting vector $S_c$ (red line) is 1.95 W/μm$^2$ compared to a single mode value (blue dashed line) of 2.45 W/μm$^2$. The percentage $\alpha$ for the 2$^{nd}$ mode is 22.2%. The gray area indicates the (stretched) cavity shape.

| $a/\lambda$=0.12 $\pi$ mode standing wave effective gradient $E_a$ = 100 MV/m | TM$_{010}$ + TM$_{011}$ Bimodal Cavity | | | Pillbox A | Pillbox B | Nose-cone |
|---|---|---|---|---|---|---|
| | 1$^{st}$ harmonic alone | 2$^{nd}$ harmonic alone | 78% 1$^{st}$ +22% 2$^{nd}$ | 1$^{st}$ harmonic only | 1$^{st}$ harmonic only | 1$^{st}$ harmonic Only |
| frequency (GHz) | 11.9942 | 23.9884 | | 11.9942 | 11.9942 | 11.9942 |
| effective shunt impedance (MΩ/m) | 95.7 | 38.3 | ▲131.4 | 89.7 | 99.1 | 113.9 |
| transit time factor | 0.765 | 0.786 | | 0.768 | 0.753 | 0.758 |
| max $E_{surf}$ (MV/m) | 246.8 | 367.4 | 246.8 | 209.7 | 246.8 | 225.0 |
| max $H_{surf}$ (MA/m) | 0.327 | 0.634 | 0.350 | 0.327 | 0.298 | 0.289 |
| max $S_c$ (W/μm$^2$) | 2.45 | 10.3 | ▼1.95 | 3.75 | 3.02 | 4.20 |
| max $\Delta T$ (°K) @ 200 ns pulse length | 27.5 | 148.2 | ▼18.6 | 27.5 | 22.87 | 21.5 |
| wall loss (MW) | 1.306 | 3.263 | ▼0.95 | 1.392 | 1.262 | 1.097 |

**Table 1:** Comparison of RF parameters between an optimized bimodal cavity and single mode cavities, where effective acceleration gradient is equalized at 100 MV/m, with red/green arrows showing up/down improvements. Pillbox A has the same maximum surface *H*-field as that of the fundamental mode in bimodal cavity; Pillbox B the same maximum surface *E*-field; and the nose-cone cavity is a single-mode cavity optimized to increase shunt impedance and lower surface pulse heating using the same code.

The numerical results listed in Table 1 are normalized to an effective acceleration gradient of 100 MV/m. To achieve a higher gradient approaching 200 MV/m, the cavity material should be hard CuAg, as in Fig. 1. The geometry of the bimodal cavity is significantly different from the structure used in CuAg RF breakdown experiments [1] where the cavity geometry was pill-box-like and optimized for single mode operation at the fundamental TM$_{010}$ mode. Note that Table 1 shows our bimodal cavity to have RF properties comparable to conventional pill-box cavities even for single mode operation. With single frequency experiments such as at the SLAC X-band test facility, if the bimodal cavity made of hard CuAg is predicted to sustain 175 MV/m acceleration gradient at X-band in single mode operation, extrapolation suggests that it could be possible to approach 200 MV/m gradient by operating with two-mode superposition. As shown in Table 1, the pulsed heating temperature rise can be 32% lower and the modified Poynting vector $S_c$ 20% lower for the same acceleration gradient. In other words, naïve scaling suggests that if one assumes that pulsed heating is the major deterministic factor for RF breakdown, two-mode operation will sustain $\sqrt{1/(1-0.32)} \approx 1.21$ times a 175 MV/m single-mode gradient which

would give 212 MV/m without increasing the pulsed heating. But if the modified Poynting vector is the dominent factor, two-mode operation will sustain $\sqrt{1/(1-0.20)} \approx 1.12$ times the gradient, namely196 MV/m. Hence it is of great importance to measure RF breakdown statistics for our bimodal cavity structure, comparing single mode operation in the $TM_{010}$ with two mode superpostion using the $TM_{010}$ and $TM_{011}$ modes, and to investigate surface fatigue on cavity surfaces after prolonged pulsed heating runs. These tasks mesh naturally with the project already underway at Yale [9].

Besides high acceleration gradient and low RF breakdown rate, beam stability is also an important charateristic needed to evaluate structure design. In this regard, we point out two favorable features of our bimodal design. First, the beam aperture to fundemantal-mode wavelength ($a/\lambda$) ratio of the bimodal cavity design is at a typical value of 0.12, and for second harmonic the ratio is even higher $a/\lambda = 0.24$; these compare with an average $a/\lambda = 0.11$ for the CLIC main linac accelerating structure [6]. Hence, wakefield issues are very likely managable and the cavity design still has room to add damping features with further optimization, which deserves dedicated future investigation. Second, our bimodal cavity structure shows unique longitudinal beam dynamics features (see below). Our studies to date show that the phase acceptance can be widened while the energy spread can be reduced, as compared to the typical *fish* plot for a single mode. These features are shown in Fig. 6.

We illustrate the beam dynamics features and their potential for emittance manipluation using a hypothetical model. For this we take the example of a bimodal cavity boost linac for use with our bimodal RF gun, which we have dubbed MUFFINS (Multi-Frequency Fotoinjector Subsystem).* The conceptual design of the boost linac and bimodal RF gun are shown in Fig. 7. The linac is composed of five bimodal cavities, operated at L-band (1.3 GHz) and S-band (2.6 GHz) scaled from the design in Table 1, which supports $TM_{010}$ and second harmonic $TM_{011}$ modes. The boost linac entrance is located near the beam waist, about one meter downstream from the RF gun. The beam envelope and emittance evolution of the electron beam in a hypothetical MUFFINS-linac system are shown in Fig. 8a, with a transverse phase plot in Fig. 8b, a longitudinal phase plot in Fig. 8c, and the bunch cross section shown in Fig. 8d.

For this example, shown to illustrate beam dynamics virtues of an accelerator structure composed of bimodal cavities, the bunch charge is 0.3 nC, initial bunch length 3 ps, and initial bunch size 0.6 mm; in MUFFINS, the first harmonic $TM_{010}$ mode at 1.3 GHz has a peak amplitude of 50 MV/m on the cathode, and the second harmonic $TM_{011}$ mode at 2.6 GHz has 12.5 MV/m on the cathode. In the bimodal linac, the first harmonic $TM_{010}$ mode at 1.3 GHz has a peak axial field 50 MV/m on the axis, and second harmonic $TM_{011}$ mode at 2.6 GHz has 12.5 MV/m on the axis. Fig. 10 shows the wide range of acceptable second harmonic phase without substantial performance deterioration, illustrating the resilience of MUFFINS against phase errors and frequency mismatch, which will ease the manufacturing and control challenges that otherwise could appear formidable. This preliminary result predicts an output beam energy of 24.2 MeV, a transverse emittance of $1\pi$ mm-mrad, a longitudinal emittance of $18.7\pi$ keV-mm, and an energy spread of 0.083%, sampled 2 meters downstream.

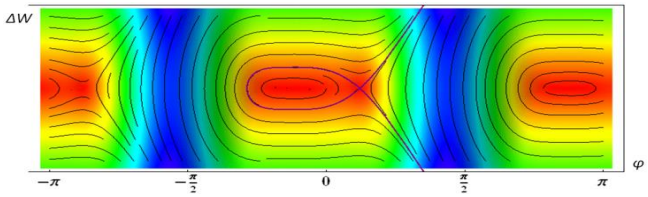


**Fig. 6:** Phase diagram for longitudinal motion, with the energy change $\Delta W$ and phase $\varphi$ relative to that of the synchronous particle, showing stretched phase acceptance and narrowed energy spread.

*MUFFINS is novel RF gun concept using 1st and 2nd harmonic RF components to suppress emittance growth, to enhance acceleration gradient, and to impede RF breakdown. MUFFINS development and design are currently supported by DoE via Phase I SBIR grant DE-SC0015158 to Omega-P R&D, Inc.

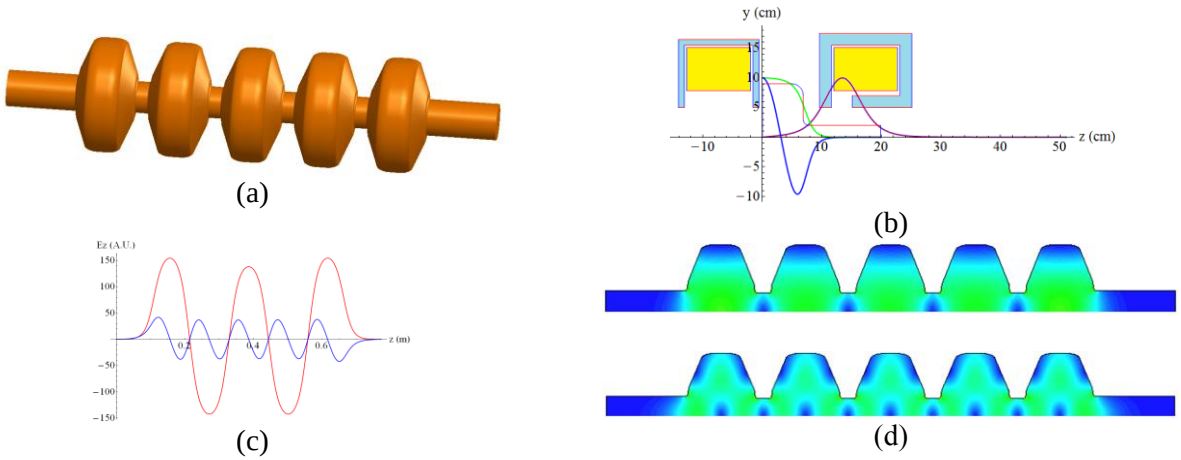


(a) (b) (c) (d)

**Fig. 7:** (a) Conceptual design of Five-cell bimodal boost linac, couplers not shown; (b) Hypothetical model of bimodal RF gun. The gun cavity profile (in red) and compensation coils are shown. The electric fields of $TM_{010}$ (green) and $TM_{011}$(blue) modes and the magnetic field (purple) of the compensation coil along the axis are plotted. (c) Longitudinal electric fields of the fundamental $TM_{010}$ mode (red curve) and its second harmonic $TM_{011}$ mode (blue), with their electric field patterns shown in (d).

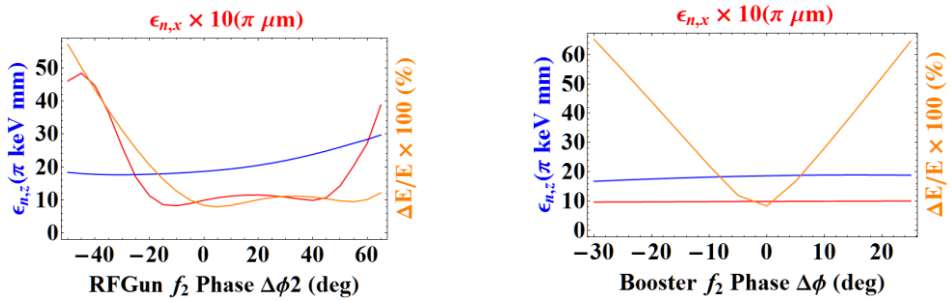


(a) (b)

**Fig. 8:** Beam characteristics at the boost-linac exit with different second harmonic RF phases (a) in the RF gun half-cell; and (b) in the boost linac. Energy spread is in orange, longitudinal emittance in blue, and transverse emittance in red.

The added versatility coming with extra degrees-of-freedom from spatiotemporal RF field manipulation in multi-harmonic cavities has raised wide interest in potential applications in accelerator physics. Similar ideas although quite different approaches have been proposed with experiments already initiated, including (1) high power RF breakdown studies of an X-band dual-moded single-frequency coaxial cavity [10], operating in a superposition of TM and TE modes; (2) emittance control in photoinjectors, using the higher harmonic frequency components to suppress the RF emittance growth shown above and in refs. [11-13]; and (3) bunch shaping in multi-frequency linacs, with two different accelerator sections at harmonic frequencies to manipulate the beam transport matrix and generate the desired ramped bunch for wakefield acceleration applications [14]. Our concept of a multi-harmonic cavity accelerator structure could embrace all the above merits with the aim of evolving into a viable accelerator structure design that can support an acceleration gradient >200 MV/m with a breakdown probability $<10^{-7}$ $m^{-1}$ per RF pulse (i.e., one event per meter structure length per 24-hour day with a 120 Hz pulse repetition rate).

Inevitably, there are bound to be technical challenges in realizing practical bimodal accelerator structures. An incomplete list of these challenges includes machining tolerance control, mechanical stability, correlated two-mode tuning, two-frequency high power RF source and RF transport systems, two-frequency coupling, and phase-amplitude locking. Some of these challenges have been confronted in our previous work [9, 15] and in the currently supported project at Yale on RF breakdown studies of bi-modal cavities; some are discussed below and have been studied further for high gradient accelerator structure

applications during Phase I. As regards the machining tolerance, machining bimodal cavities with the necessary tight dimensional tolerances should be possible using recently described techniques that maintained dimensions to within 5 μm [16]. Further evidence for precision tuning of a not-dissimilar bimodal cavity has also been reported [15]. Our preliminary study of beam dynamics in a bimodal cavity structure shows that there is a rather wide range of phase acceptance for beam stability, which should ease the stringent requirements of tolerances and frequency detuning.

A bimodal cavity accelerator as described here would be built using conventional RF technology, not dissimilar from that required for CLIC structures. Thus its stageability, beam transportation technology, and positron acceleration capability would be direct descendants of currently mature RF accelerator technology. Further, for any high gradient accelerator concept, the chance of ever evolving into a main acceleration mechanism for a future multi-TeV collider depends highly on it possessing a high-wall-plug-to-beam power efficiency. The capability of RF-based accelerators is highly constrained by the availability, performance, and efficiency of high power RF sources; and in this connection a bimodal cavity accelerator would be no exception. However, bimodal cavity accelerator can improve RF-to-beam efficiency (and hence wall-plug-to-beam efficiency), as compared to single mode operation, because (a) the effective shunt impedance is increased as shown in Table 1, since the total power consumption for two modes is quadratically dependent on the second mode percentage; and (b) the cavity filling time is shorter for the higher frequency component, so less energy is wasted upon filling the cavity. For the same bunch structure as the CLIC main linac [17], we compare in Table 2 the performance of cavity structures in single mode or bimodal operation. Also listed in Table 2 are parameters of the CLIC DDS A structure [17], which is a damped and detuned accelerator structure for the main linac of CLIC. For the plain design without additional damping features, the bimodal cavity structure in two-mode operation has a 30% RF-to-beam efficiency, and requirement for a considerably lower level of RF drive power.

| gradient $E_{0T}$=105 MV/m, $q_b$=0.64 nC, $t_s$=0.5 ns, $t_b$=156 ns, $t_p$=250 ns | single mode | bimodal | | CLIC_DDS_A |
|---|---|---|---|---|
| | | X-band | K-band | |
| unloaded quality factor $Q$ | 8573 | 8573 | 9713 | 5020 ~ 6534 |
| coupling factor $\beta$ | 2.17 | 2.50 | 7.69 | |
| filling time $t_f$ (ns) | 71.8 | 65.1 | 14.8 | 45.4 |
| shunt impedance $R'$ (MΩ/m) | 95.7 | 131.4 | | 51 ~ 118 |
| pulsed heating ΔT (°K) | 33.9 | 22.9 | | 51 |
| Poynting vector $S_c$ (W/μm$^2$) | 2.70 | 2.15 | | 6.75 |
| rf input power (MW/m) | 250 | 175 | 43.5 | 354 |
| rf-to-beam efficiency $\eta_{rf\text{-}beam}$ (%) | 24.3 | 30.0 | | 23.5 |

**Table 2:** Performance of a cavity structure in single mode or bimodal operation compared with CLIC_DDS_A structure. Effective acceleration gradient is 105 MV/m, and CLIC bunch structure is used, with $4 \times 10^9$ electrons per bunch, bunch separation 0.5 ns, total bunch train of 156 ns, and RF pulse length of 250 ns. More favorable values for all five of the last parameters are predicted for the bimodal cavity structure, as compared with single mode or with the cited CLIC structure.

| $t_s$=0.5 ns, $t_b$=156 ns, $t_p$=250 ns | Case 1 | Case 2 | Case 3 | Case 4 | Case 5 |
|---|---|---|---|---|---|
| bunch charge (nC) | 0.64 | 0.64 | 0.64 | 1.28 | 0.32 |
| effective gradient $E_{0T}$ (MV/m) | 105 | 50 | 200 | 200 | 200 |
| input power $P_{g1}$ and $P_{g2}$ (MW/m) | 175 44 | 66 17 | 454 107 | 654 163 | 354 79 |
| rf-to-beam efficiency $\eta_{rf\text{-}beam}$ (%) | 30 | 41.7 | 19.7 | 30.8 | 11 |

**Table 3:** Performance of bimodal cavity structures with different gradient and bunch charge, where bunch separation 0.5 ns, total bunch chain 156 ns, and RF pulse length 250 ns.

Scenarios for operation of bimodal cavity accelerator structures have been examined, with results in Table 3, suggesting that an overall wall-plug-to-beam efficiency of about 10% could be achieved as in Case 4, based on use of a bimodal cavity accelerator structure that we predict can have 30% RF-to-beam efficiency.

In conclusion, this introductory exposition shows the potential benefits of a bimodal accelerator structure, including the higher acceleration gradient, smaller footprint of the accelerator complex, higher beam quality, higher RF-to-beam efficiency, and possible efficiency and cost savings for the overall accelerator system. These benefits should well outweigh the cost of an additional RF power source or frequency multiplier and associated complexity of a two-frequency system.

## III. RESULTS OF WORK ON PHASE I TASKS

Technical feasibility has been demonstrated during Phase I that provides a well-founded basis for a successful Phase II project, as described in this section. The technical objectives of the Phase I project—as they were proposed—are listed below, in *italics*, with progress then described for each objective.

*(1) To optimize cavity design, including improving Q factor, shunt impedance, transit time factor, and RF-to-beam energy transfer efficiency. Algorithms will be developed to enhance the simulation capability, especially for multi-frequency analysis.*

The geometry of multi-harmonic cavities has been simplified and parameterized and the sensitivity of each RF property to variations in each geometrical parameter has been analyzed, as shown in Fig. 9. For reference, typical values of the parameters as defined in Fig. 9a are $l = \lambda/2$, $d = 0.88\lambda$, and $g = 0.2\lambda$, where $\lambda$ is the wavelength of the fundamental mode; so for an S- and C-band cavity, $l = 5.25\ cm$, $d = 9.24\ cm$, and $g = 2.1\ cm$. The frequency response for each mode to each geometric perturbation is different and not linearly correlated to other parametric perturbations; hence it is possible to tune each frequency to a desired value with small effects on other RF properties. Several strategies were applied to optimize the cavity geometry. First, *Genetic Algorithm* was applied to explore the whole parameter space with weighted target functions on the overall RF properties. Once a candidate was found satisfying the desired conditions (e.g. $E_g$), *multivariate optimization* was applied to fine tune some selected parameters to achieve desired frequencies while constraining the other RF properties within certain ranges. Several iterations of optimization were performed until both cavity frequencies and other RF properties reached desired values. The sensitivity of frequencies can serve as guidance for defining machining tolerances.

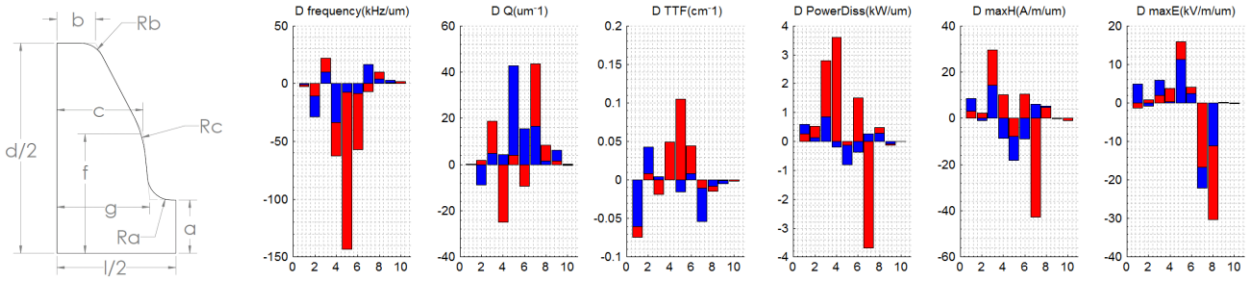


(a) (b)

Fig. 9. (a) Geometrical parameterization of a two-harmonic cavity. (b) Sensitivities to geometric perturbations of RF cavity frequency, quality factor, transit time factor, power dissipation, maximum surface magnetic and electric fields. Blue bars are for fundamental, and red for second harmonic. Horizontal axis numbers correspond in order to parameters *l, d, a, b, c, f, g, Ra, Rb,* and *Rc,* defined in Fig. 9(a).

*(2) Based on the preliminary optimization results, design a multi-cell bimodal cavity structure aiming to support very high gradient and very low RF breakdown rate.*

A structure comprising bimodal cavities operating at S-band (2.856 GHz) and C-band (5.712 GHz) was selected, since these are the frequencies of a multi-MW source at Yale available to Omega-P R&D [9]. A five-cell structure was selected that includes end cells, nominal cells, and a coupling cell. This is to demonstrate our full-range design capability and to meet project objectives. The design method can be extended to different frequency bands and to higher cell number, as shown in Fig. 10b.

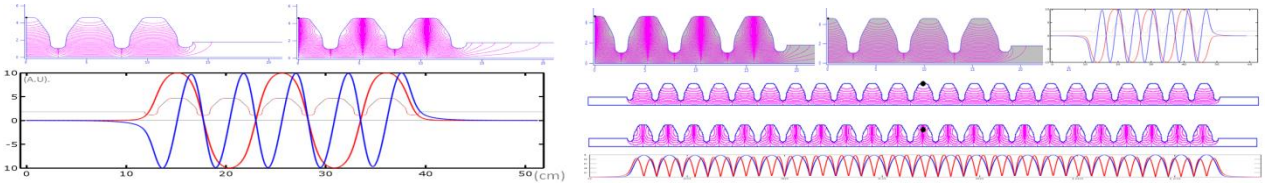


(a) (b)

Fig. 10. Multi-Cell Multi-Harmonic Structure with axial field flattened for both harmonic modes. Red field strength curves are for S-band, and blue curves for C-band

We designed the new bimodal coupling scheme shown in Fig. 11 for the multi-harmonic cavity. S- and C-band couplers, located at opposite sides of the cavity with similar dimensions—as for a dual feed system—so as to compensate for field distortions. The S-band coupler to excite the $TM_{010}$ mode has a conventional waveguide slot design. The C-band coupler to excite the $TM_{011}$ mode uses two symmetric coupling apertures to feed second-harmonic power in opposing phases. Due to the mirror symmetry at the mid-plane of the cavity, the second-harmonic field cancels at the S-band coupling aperture; hence there is negligible C-band leakage into the S-band waveguide; this is confirmed in Fig. 11d. This design concept avoids an RF choke in the S-band waveguide; hence the C-band power is localized inside the cavity without building up field enhancement at a choke region. The peak surface field remains similar to that of the cavity without a coupling aperture, and there is no severe field enhancement around the coupling aperture. The insertion of waveguide input couplers detunes the cavity resonance frequency, requiring careful re-tuning of the coupler cell. With the proper rescaling of boundary conditions and coupling coefficient, we have found that the coupler cell can be simulated alone before integration into the full structure..

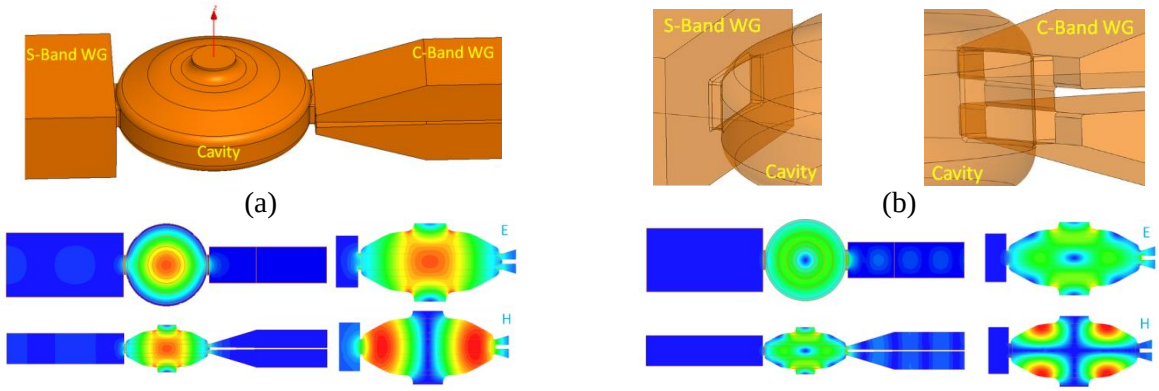


(a) (b)

(c) (d)

Fig. 11(a). Design of couplers for a bimodal harmonic cavity; (b) detailed view of the coupling apertures; (c) patterns for *E* and *H* fields of S-band power excitation; and (d) of C-band excitation.

For multi-cell structures, an important issue is to tune the axial field flatness in order to ensure the desired mode excitation, to maximize the net accelerating voltage, and to minimize the peak surface fields. As a provisional technique in advance of that we will employ for Phase II structure cold tests, a virtual bead-pulling experiment and its associated algorithm were designed and carried out to "measure and tune" field flatness. A small metallic sphere moving along the structure center axis was introduced in RF

simulations; frequency deviations were recorded as measures of local field strength; perturbation theory[18] was then used to calculate the local cell detuning. For a conventional single-mode cavity, one only needs to push or pull one tuning pin per cell to achieve the desired detuning. But for a bi-harmonic structure, detuning of both frequencies must be corrected. A similar method discussed for single-cell optimization was used to determine a combination of geometrical perturbations required to tune both frequencies. Fig. 12 shows application of this algorithm. A small perturbation on the geometry, such as a coupler slot, results in a non-flat axial field,. The algorithm was applied to tune the frequencies and achieve field flatness, as shown in Figs. 12c and 12d, where up to 80 iterative steps were taken to achieve field flatness. Fig. 13 shows the scattering parameters $S_{11}$ of the tuned structure for each mode. The frequencies of the near-by $4\pi/5$ mode are seen to be well separated from the design $\pi$ mode.

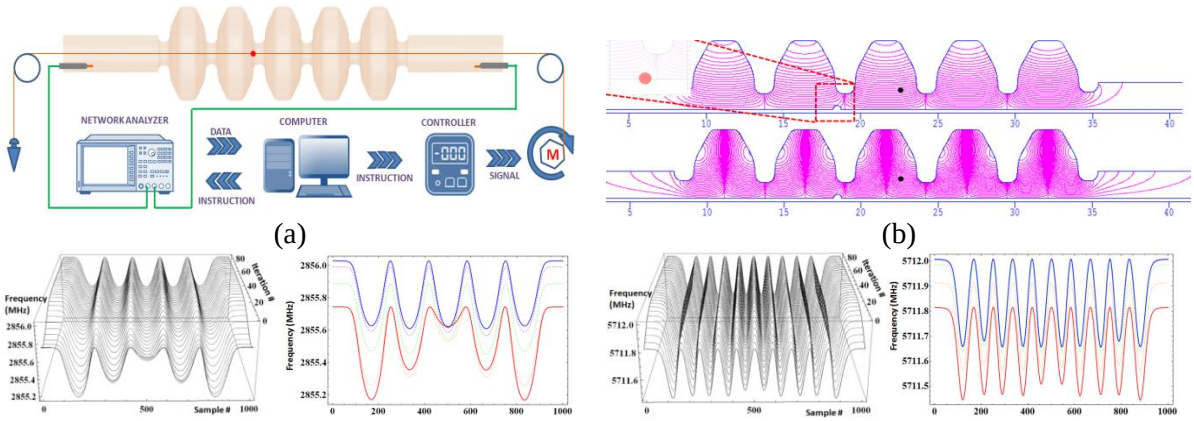


Fig. 12. (a) Schematic of a bead pulling experiment; (b) a virtual bead pulling experiment using SUPERFISH to tune the multi-harmonic cavity. In (c) and (d) red curves indicate the initial frequency deviation and axial field unevenness, and blue curves show the results after applying the tuning algorithm iteratively, while the dashed curves indicate up to 80 converging intermediate steps.

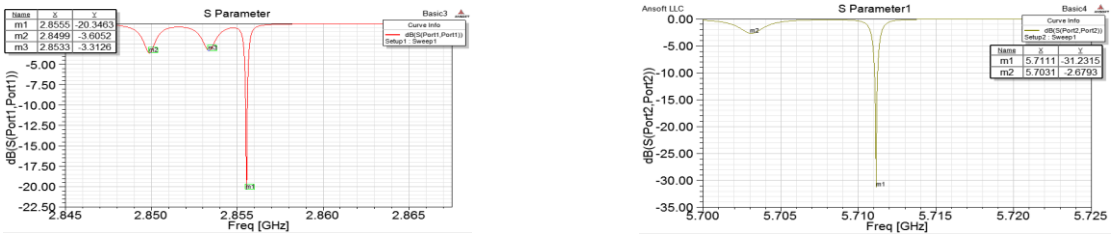


Fig. 13. Scattering parameter $S_{11}$ for (a) S-band and (b) C-band waveguide coupling to the structure.

*(3) Further optimize the structure choice based on wakefield and beam dynamic simulations. Means for suppressing unwanted higher order modes will be investigated. Extensive wakefield simulation and beam dynamic simulations could shed light on the beam stability using the MHC structure.*

Wakefields and beam dynamics behavior are directly influenced by structure geometry. Accordingly, we have considered means to minimize structure asymmetry caused by RF couplers. Our previously proposed coupler design was to feed each cavity individually with both waveguides opening to the side wall of each multi-harmonic cavity. However, we are concerned that asymmetric couplers will distort the RF field distribution and induce undesired beam dynamics issues. Hence the cavity design is simplified to use a single coupler cell at the center of structure with a dual feed coupler design as shown in Fig. 11. The multi-harmonic cavity structure is to be composed of four quadrants that will allow for HOM damping in slots between each quadrant, as in a CLIC open structure [19].. Such axial cuts along the structure will not interrupt surface currents, will allow easy assembly and disassembly of our structure for tuning and re-

machining if necessary, since no brazing of the quadrants to one another is necessary. The four quadrants will be clamped together externally without brazing, a favorable arrangement for structures made of hard-copper or copper alloy [1] that have been shown to exhibit superior breakdown-resistance. Precise positioning is to be secured by multiple dowel pins. A coolant path for thermal control of the structure can be easily integrated into each quadrant. The test structure will be high-vacuum compatible but not itself vacuum tight, since it will be operated within a large vacuum test cell for our proposed experiments. The structure will be encased in a heating shroud for bakeout and thermal tuning.

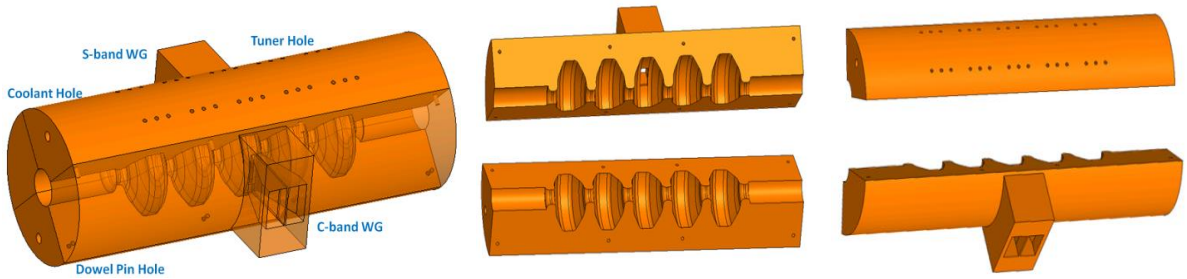


Fig. 14. Four-quadrant bimodal harmonic cavity accelerator structure concept using our new coupler design. The quadrants can be clamped together without brazing, thus allowing disassembly for dimensional adjustments as needed.

Wakefield simulation of this structure was carried out using *ABCI*; only short-range wakefields have so far been studied. Results are shown in Fig. 15. For a longitudinal bunch size $\sigma$ = 1 mm, the monopole longitudinal wake loss factor was found to be 3.5 V/pC per cell; the dipole transverse wake loss factor to be 53 V/pC/m per cell, and the dipole longitudinal wake loss factor to be 37 kV/pC/m$^2$ per cell; all are within the typical range for S-band accelerator structures [20,21].These results are for a beam aperture to wavelength ratio $a/\lambda = 0.1$ with $\lambda$ = 105.04 mm, the S-band wavelength. We have studied longitudinal beam dynamics in a similar multi-harmonic cavity structure for an RF gun design as described on pp. 6-7. The uncommon spatio-temporal RF field distributions in multi-harmonic cavities allow manipulation of the phase space of the accelerated beam while providing high acceleration gradient with low breakdown rate.

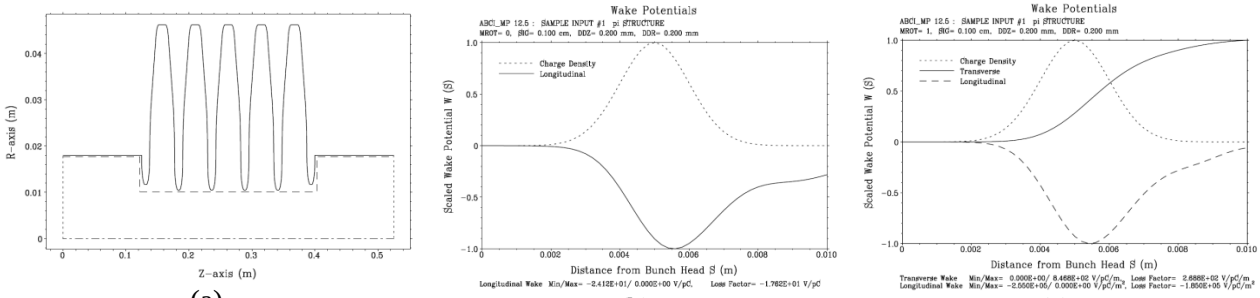


(a) (b) (c)

Fig. 15. (a) Geometry for multi-harmonic cavity wakefield simulations with a bunch size $\sigma = 1$ mm; (b) short-range wake for monopole field; and (c) for dipole field.

Fig. 16 shows some beam dynamics results. Fig. 16(a) is a map of the dependence of energy gain on the phase of the two harmonic components on bunches with 6 MeV initial energy after having passed through the 5-cell multi-harmonic cavity structure; for this example the effective acceleration gradient was 20 MV/m with 22% contribution from the 2$^{nd}$ harmonic. One sees a wide phase acceptance window for the 2$^{nd}$ harmonic component. Fig. 16(b) shows a map of the acceptance window for various initial bunch energies and 1$^{st}$ harmonic phases with the relative 2$^{nd}$ harmonic phase fixed.

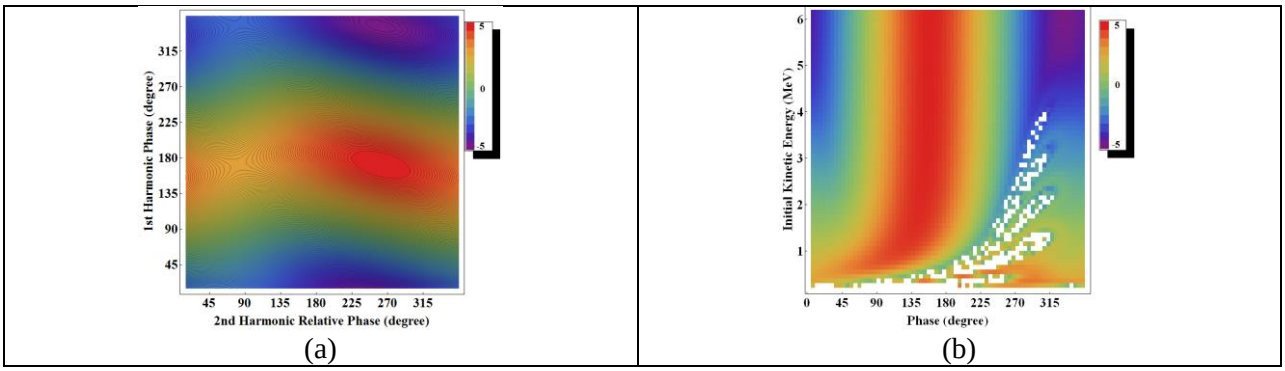


Fig. 16. (a) Map of energy gain in MeV versus phases of the two harmonic components. (b) map of acceptance window versus initial energy and 1st harmonic phase, with the relative 2nd harmonic phase fixed. Blank regions indicate the parameter space where the beam is reflected.

*(4), (5) and (6): Design a mockup cavity based on optimized dimensions with provision for two-frequency coupling, good vacuum pumping and for appropriate diagnostics at low power; develop a tuning mechanism with tuning pins to achieve the two desired cavity resonance frequencies at the fundamental and second-harmonic; and build the mockup cavity and carry out non-vacuum cold tests of candidate cavity design with bead pull experiment. If necessary, should cold-test results be unsuitable, design adjustments will be made, and the tests repeated.*

Due to delays of coupler machining and time constraints, only a mockup single-cell cold-test structure without a coupler was built and tested. This structure had a radial cut instead of axial cuts. For our S-band cavity with $a/\lambda = 0.1$, good vacuum pumping will be ensured. The main objective of our mockup cavity test was to demonstrate feasibility of designing and building a bimodal harmonic cavity with a practical tuning mechanism. With modern machining and simulation technology, we found the discrepancy between design and fabricated outcome to be sufficiently small. We found that fine tuning of mode frequencies can be achieved by means of push/pull tuning pins at different positions, as shown in Fig. 17. $TM_{010}$ and $TM_{011}$ modes have different field distributions, and so have different sensitivities to wall deformations, according to the Slater theorem [21]. In our cold tests, instead of actually deforming the cavity wall, we used small protruding screws at strategic locations to allow lowering cost, expediting the machining, and use of aluminum rather than copper. Fig. 17 shows that, by adjusting the protruding length of the screws, both harmonic frequencies could be tuned within an accuracy of 15 kHz to the desired values. An additional means to tune is by temperature regulation of the entire structure. For our four-vane structure, another possibility is to adjust the spacings between quadrants as exploited in a W-band open structure [3]. A beam-pulling experiment was conducted on this single-cell structure, with the results shown in Fig. 18, in excellent agreement as seen with the simulation results.

*(7) and (8): Design experiments to be carried out during Phase II in order to measure the acceleration gradient and RF breakdown statistics in a multi-harmonic accelerator structure; and finalize the multi-harmonic accelerator structure design and create engineering drawings for fabrication of the structure to be tested at high power in the Phase II proof-of-principle experiments.*

The main technical objective for this project is to show that a multi-harmonic cavity accelerator structure can support high acceleration gradients while the RF breakdown probability and surface damage due to surface pulsed heating can be lowered. Planned proof-of-principle experiments to be conducted during Phase II will involve excitation of the accelerator structure cavities in the $TM_{010}$ mode at S-band and in the $TM_{011}$ mode at the 2nd harmonic in C-band; to confirm its high gradient performance; and to study its RF breakdown and surface pulsed heating. A schematic of the experimental setup to measure acceleration gradient and pulsed temperature rise and to register RF breakdown events is shown in Fig. 19. High power phase synchronous RF powers at 2856 and 5712 GHz are generated by the klystron and 2nd-harmonic multiplier.

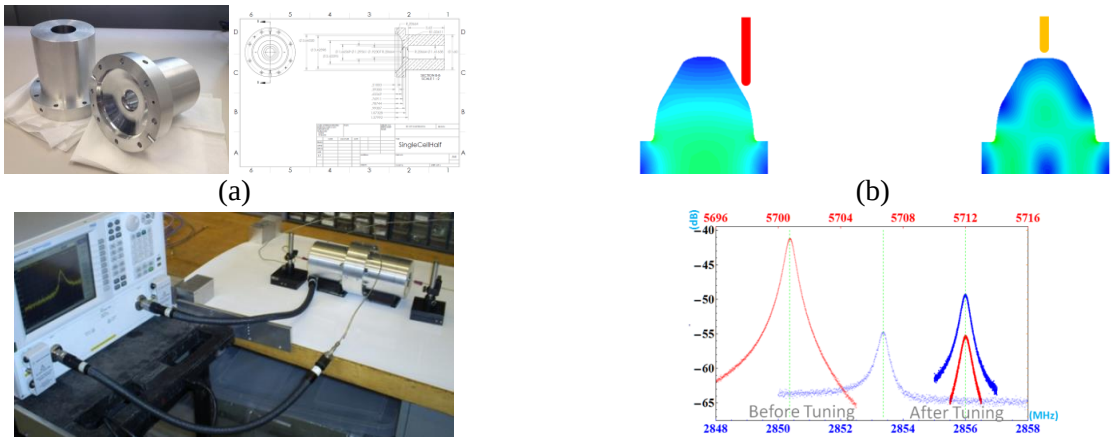


Fig. 17. (a) Mockup cavity that was cold tested, and its engineering drawing; (b) tuning screw positions; (c) experimental setup for mockup cavity two-frequency tuning; and (d) tuning results that show both harmonic frequencies tuned to the desired values, within 15 kHz.

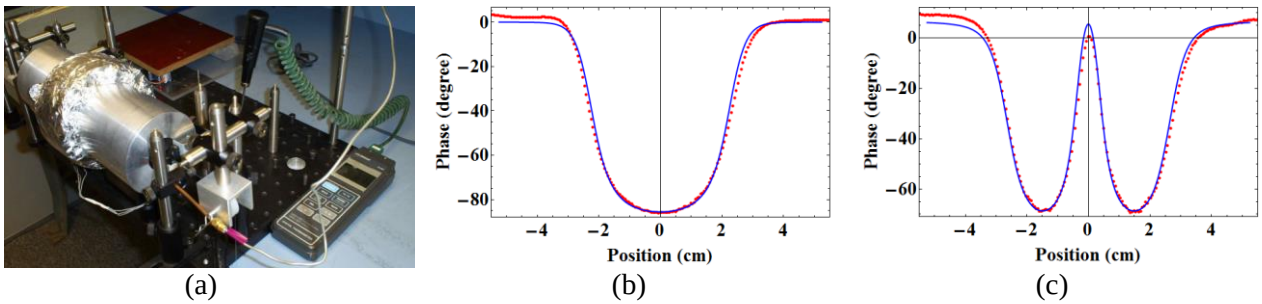


Fig. 18. (a) Experimental setup for bead-pull tests on the bi-harmonic cavity structure; (b) plot of RF transmission phase $\phi$ versus bead position for the fundamental $TM_{010}$ $\pi$-mode, where red dots are the experimental data and blue curve is based on $(f - f_0)/f_0 = \tan \Delta\phi \,/2Q$ with $f$ simulated using virtual bead pulling method as in Fig. 12; (c) phase $\phi$ versus bead position for the 2nd harmonic $TM_{011}$ $\pi$-mode.

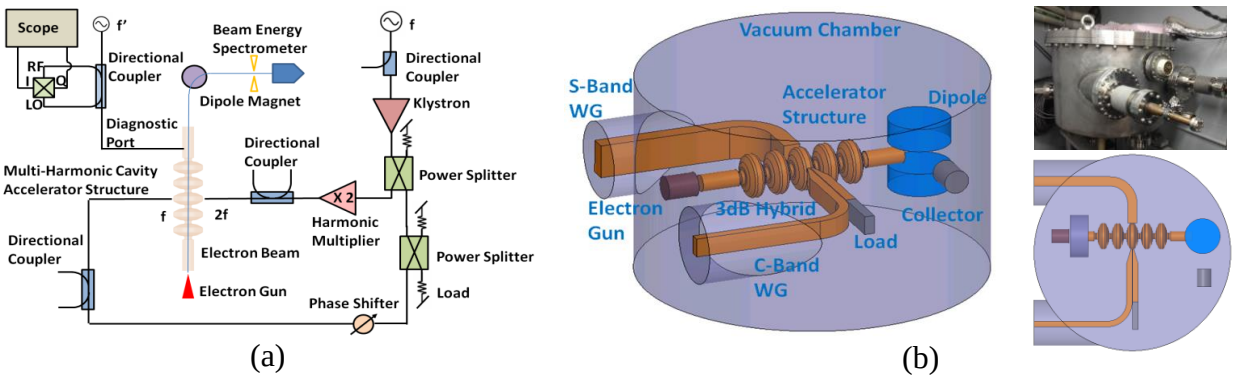


Fig. 19. (a) Experimental schematic to measure acceleration gradient, pulsed temperature rise, and cavity *Q*; and to register RF breakdown events in our bimodal harmonic cavity. (b) layout of the experiment inside a 30" diameter vacuum chamber.

The proposed S- and C-band structure is to be a scaled-up version of X- and K-band structure listed in Table 2. Normal conducting cavity RF power dissipation scales as the inverse square-root of RF frequency, hence the power requirement for achieving an effective acceleration gradient of 150 MV/m for

an S- and C-band single cell cavity is within the capability of our single XK-5 S-band klystron capability of 24 MW without need of RF pulse compression. Single-cell bimodal cavity RF breakdown experiments are currently supported at Yale by DoE under grant DE-SC-00010699. For our S- and C-band five-cell structure described here, the target gradient to be expected will be about 60 MV/m. This gradient can be achieved by S-band excitation alone, or by multi-mode excitation (which only requires <75% power of the S-band-alone case); and the RF breakdown rate and surface damage can be compared to results of the single cell experiments. Once the Phase II goals given below in Section IV are met, a future upgrade could include constructing S- and C-band RF pulse compressors with compressor efficiency 75% and power gain of 6.7:1 to reach an effective acceleration gradient of 150 MV/m; and/or a power gain of 11:1 for 200 MV/m. For our five-cell structure with each cell 5.2 cm in length (equivalent to π phase advance in an S-band accelerator structure), running for about one 24-hour day at a 10 Hz pulse rate can allow accumulation of RF breakdown statistics valid in the range of $10^{-5}$/m. Variations in cavity $Q$ can indicate long-term cavity $Q$ degradation to determine permanent surface damage. As the test accelerator is a clamped structure with four demountable quadrants, visual inspection and SEM examination after high power tests can be conveniently performed, to reveal location and seriousness of any surface damage.

Fig. 20 shows the C-band input waveguide network, which is composed of a 3-dB hybrid and a phase delay line to deliver two equal amplitude second harmonic components having opposite phases. Currently this is a proof-of-concept design; the final design will optimize the dimensions to fit inside the vacuum chamber.

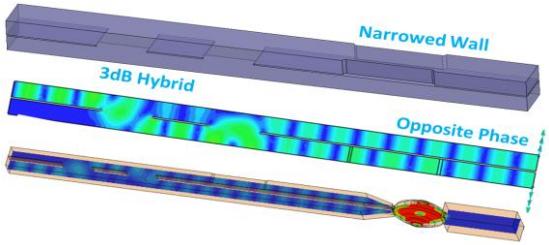


Fig. 20. C-band 3-dB E-plane coupler with π-phase shift section. Input to bimodal cavity is at right side.

Fig. 19 shows a moderate energy electron gun inside the vacuum test cell to provide a low-current test beam to traverse the structure, with its final energy distribution analyzed by a spectrometer to infer acceleration gradient. Predictions for this technique are shown in Figs. 16 and 21. Use of a low energy un-bunched beam, chosen for simplicity, is only valid for small acceleration gradients that will be realized by lowering the RF drive powers; otherwise significant reflections of the test beam can occur. Such measurements benchmark against predictions based on the simulations, and allow scaling to predict gradients at higher RF powers.

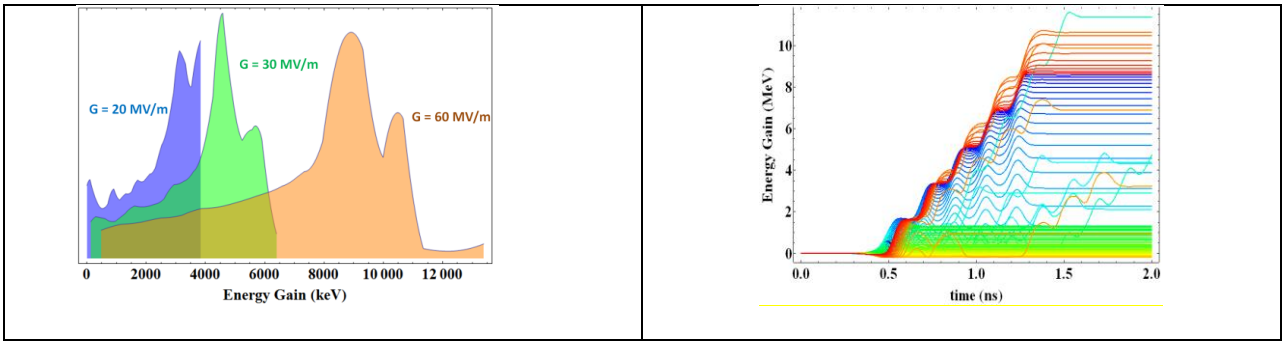


Fig. 21. (a) Final energy distribution for a 200 keV unbunched electron beam passing through our 5-cell multi-harmonic cavity for different acceleration gradients.
(b) energy gain versus time for the acceleration gradient = 60 MV/m case, for different injection phases.

An additional diagnostic we plan to use to assess cavity changes due to pulse heating and breakdown involve online measurements of cavity *Q*. Because electrical resistivity depends on the surface temperature and surface condition, the cavity *Q* will change when the cavity surface is heated or damaged during high-power pulsing. By using a diagnostic cavity mode at a frequency above 5712 GHz and at low RF power, coupling changes to the diagnostic mode will be observed when cavity *Q* is changed. By measuring the change in the amplitude and phase of the reflected power from the diagnostic mode using an IQ demodulator to determine the dynamic *Q* change, the temperature rise on the certain area of the cavity surface can be deduced based on simulated field pattern of this diagnostic mode [9]. Beam pipe openings or small gaps between quadrants of the structure can serve as the diagnostic ports, for example. Excessive reflected power will indicate the occurrence of RF breakdown. The amplitude ratio and phase relationship between the two high power harmonic components will be varied to study the effects of different spatio-temporal distributions of the electromagnetic fields on gradient and RF breakdown properties.

Fig. 19 shows our planned experimental test setup in the Yale Beam Physics Lab, and a diagram of the experimental arrangement. All critical elements will be positioned within an existing 30" diameter cylindrical vacuum chamber left over from earlier active RF pulse compression experiments [22]. This chamber will be positioned in the lab just adjacent to the two-frequency multi-MW RF source. In addition to the RF elements, Fig. 19 also shows a moderate-voltage electron gun to provide a test beam to measure acceleration gradient in the structure, and an analyzing dipole magnet. The cover of the vacuum chamber can be lifted to allow convenient installation and adjustment of the individual elements. Evacuation of this chamber is effected by two existing 400 l/s ion pumps with associated power supplies. The electron gun for measurement of acceleration gradient is also available; details of this diagnostic are discussed below. The dipole magnet for analyzing the beam energy distribution will be built following standard designs using vacuum compatible wiring. A heating shroud (not shown in the drawing) for bake-out of the structure and associated elements will be installed to allow preliminary vacuum conditioning. This shroud can also be used for thermal tuning of the structure, insofar as temperature increases will suffice.

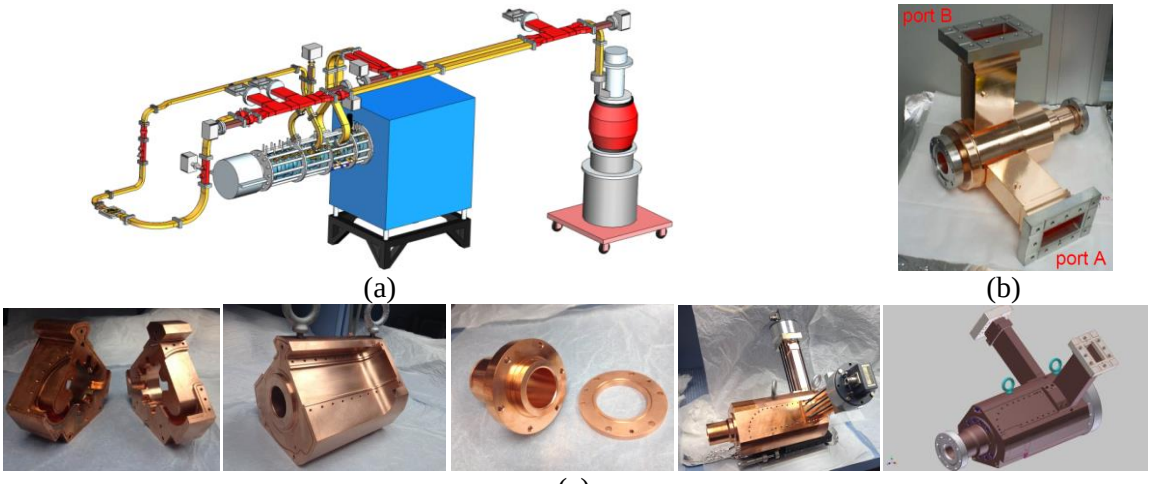


Fig. 22. (a) Layout of Yale dual-frequency RF source, here shown feeding a bimodal test cavity; (b) the fabricated S-band drive cavity, after tuning and prior to installation; (c) parts during assembly of the C-band 2nd harmonic output cavity. The vacuum test cell containing the bimodal harmonic cavity accelerator structure will be positioned at the left side of the source oriented as in Fig. 22a, with the C- and S-band waveguides aligned with the input waveguides of the test cell, as shown in Fig. 19.

The most significant Yale facility for the Phase II experiments is the dual-frequency RF source [9], sketched in Fig. 22. Here, S-band power from an XK-5 SLAC klystron is divided, with a portion driving

a $TE_{111}$ rotating mode cavity to provide cyclotron resonance acceleration of an injected 250 keV 20-A beam. This beam traverses a $TE_{211}$ rotating mode cavity where it efficiently generates second-harmonic C-band power that is phase synchronous with the S-band power. The waveguide layout allows for continuous adjustment of the relative amplitude and phase of the two high powers.

The 2nd harmonic rotating $TE_{211}$ mode output cavity proved to be a challenge to fabricate, due to design requirements that included rounded output ports and balancing protrusions to minimize field enhancements and maintain field symmetry. Two major machine shops that routinely fabricate test accelerator structures for US National Labs failed in their attempts to machine the parts for this structure. Finally, a shop hired previously for other Yale projects, located nearby in Oxford, CT, succeeded with this daunting task. Cold tests of this 2nd harmonic cavity have been carried out, as shown in Fig. 23. This figure shows the cavity connected to the available vector network analyzer, the S parameters, and a drawing of the cavity. Fig. 23b shows the two degenerate orthogonal $TE_{211}$ modes to have eigen-frequencies that are by design about 17 MHz lower than the nominal operating frequency of 5.712 GHz;; this difference is being corrected by thinning by about 2 mm the tuning ring shown in the central photo in Fig. 23c. After confirming desired tuning change, the 2nd harmonic cavity will be vacuum brazed.

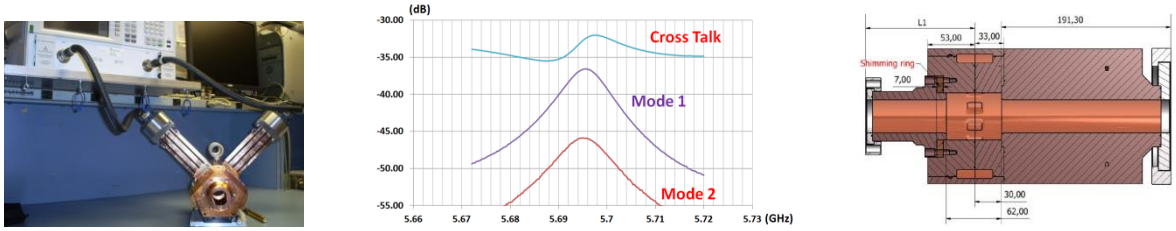


(a) (b) (c)

Fig. 23. (a) Mode frequency measurement in C-band output cavity before fine tuning; (b) S-parameter measurement results, for the two degenerate $TE_{211}$ modes with different polarizations as required to couple and comprise a rotating mode. Frequency tuning to 5.712 GHz from 5.695 GHz shown is being done by thinning the tuning shim ring that is shown in the central photo in Fig. 22(c).

Operation of the S-band drive cavity, shown in Fig. 24a, was under conditions found in simulation studies of the 2nd harmonic cyclotron resonance frequency multiplier. Fig. 24b shows a trace of the 110-kV, 7-A current pulse collected downstream from the drive cavity, as interrupted by application of RF power (blue trace) with pulse structure shown in red. Full current interruption to the 45-mm diameter collector is consistent with beam cyclotron acceleration from 110 to about 250 kV. Operation of the 2nd harmonic RF source is designed for a 250 kV, 20 A injected beam, with cyclotron acceleration up to 700 kV.


(a) (b)

Fig. 24. (a) harmonic multiplier drive cavity installed in the magnet system, connected to the electron gun tank (at left) and the dual feed RF network; and (b) results of collector beam current measurement using beam-interruption method to infer transverse beam acceleration in the drive cavity.

## IV. SUMMARY

Exposition is now complete of results obtained during Phase I to fulfill its stated objectives. The Phase I study has deepened understanding of operation of an accelerator structure comprising bimodal harmonic cavities we predict can sustain an acceleration gradient approaching 200 MV/m with a breakdown rate < $10^{-7}$ $m^{-1}$. Results include means for designing bimodal cavity structures, coupling power into the structure at the two frequencies, tolerance sensitivities to variations in all 10 cavity geometrical parameters, influence of wake fields on beam dynamics, design of a demountable clamped structure with minimal braze joints, and design of a vacuum test cell containing the test accelerator structure and diagnostics. These results constitute a solid basis for success in the Phase II project.

## V. BIBLIOGRAPHY AND REFERENCES CITED


1. Sami Tantawi, "Linac Technology for Compact Sources," Qatar Foundation Compact X-Ray Light Source Workshop, April 4-5, 2014
2. Sami Tantawi, "Advanced high frequency acceleration, high repetition Rate linacs and RF undulators," , 15th IEEE International Vacuum Electronics Conference, Monterey, California (2014)
3. M.D. Forno, V. Dolgashev, G. Bowden, C. Clarke, M. Hogan, D. McCormick, A. Novokhatski, B. Spataro, S. Weathersby, and S. G. Tantawi, "RF breakdown tests of mm-wave metallic accelerating structures," Phys. Rev. Accel. Beams 19, 011301 (2016); and references therein.
4. M. Aicheler, P. Burrows, and et al (ed.), "A multi-TeV linear collider based on CLIC technology: CLIC conceptual design report," CERN-2012-007 (2012)
5. V. Dolgashev, S. Tantawi, et al, "Geometric dependence of radio-frequency breakdown in normal conducting accelerating structures," Appl. Phys. Lett. 97, 171501 (2010); and references therein.
6. A. Grudiev, S. Calatroni, and W. Wuensch, "New local field quantity describing the high gradient limit of accelerating structures," Phys. Rev. ST Accel. Beams, 12, 102001 (2009).
7. A. Grudiev and W. Wuensch, "Design of an X-band accelerating structure for the CLIC main linac," Proceedings of LINAC08, Victoria, BC, Canada THP062, pp. 933-935 (2008)
8. S.V. Kuzikov, S.Yu. Kazakov, Y. Jiang, and J.L. Hirshfield, "Asymmetric bimodal accelerator cavity for raising RF breakdown thresholds," Phys. Rev. Lett. 104, 21480 (2010).
9. Y. Jiang, S.V. Kuzikov, S.Yu. Kazakov, J.L. Hirshfield, "Multi-harmonic test setup for RF breakdown studies," Nucl. Instr. and Meth. Phys. Res. A, Volume 657, p. 71-77 (2011)
10. F. Wang, C. Adolphsen, C. Nantista, "Initial high power test results of an X-band dual-moded coaxial cavity," Proc. 2011 Particle Accelerator Conf., paper TUP139.
11. L. Serafini et al., "Neutralization of the emittance blowup nduced by the RF time dependent forces in RF guns," Nucl. Instr. and Meth. A 318, pp. 301-307 (1992)
12. D.H. Dowell and et al, "A two-frequency RF photocathode gun," Proc. of 25th International Free Electron Laser Conference (FEL 2003), SLAC-PUB-10851.
13. J.-Y. Raguin, R. J. Bakker, K. Li, M. Pedrozzi, "A two-frequency RF cavity for the psi low emittance gun," Proceedings of the 27th IFEL Conference, 324 (2005).
14. P. Piot and et al, "Generation and characterization of electron bunches with ramped current profiles in a dual-frequency superconducting linear accelerator," PRL, 108, 034801 (2012)
15. Y. Jiang and J. L. Hirshfield, "Multi-harmonic accelerating cavities for Rf breakdown studies," Proceedings NA-PAC2013, Pasadena, CA, WEPMA28, pp.1040-1042 (2013)
16. S. Atieh, M. Aicheler, and et al, "Machining And characterizing X-band RF-structures for CLIC," Proceedings IPAC2011, San Sebastián, Spain, TUPS098, pp.1768-1770 (2011).
17. V. Khan, "A damped and detuned accelerating structure for the main linacs of the compact linear collider," EuCARD-BOO-2011-001 (2011)
18. H. Padamsee, J. Knobloch, T. Hays, RF Superconductivity for Accelerators, ISBN-10: 3527408428, Publisher: Wiley-VCH (1998)
19. H. Zha, A. Grudiev, V. Dolgashev, Optimization of CLIC-G structure & Design of CLIC open structure, CLIC Workshop 2016, CERN (2016).
20. K.L.F. Bane, Wakefield effects in a linear collider, AIP Conf. Proc. 153, 972-1014 (1989); P.Wilson, Wakefield and wake potentials, AIP Conf. Proc, 184, 526-564 (1989).
21. Thomas Wangler, *RF Linear Accelerators* (2nd ed.). Wiley-VCH. ISBN 978-3-527-62343-3 (2008).
22. O. A. Ivanov, A. A. Vikharev, A. M. Gorbachev, V. A. Isaev, M. A. Lobaev, A. L. Vikharev, S. V. Kuzikov, J. L. Hirshfield, and M. A. LaPointe, Active quasioptical Ka-band rf pulse compressor switched by a diffraction grating, Phys. Rev. ST Accel. Beams 12, 093501 (2009).